Modifying aluminum phthalocyanine with quantum dots to promote cellular uptake and enhance the efficacy of anticancer photodynamic therapy

Li Lei[1], Bin Dai[2], Ting Han[3], Cheng Zhou[2], Zhao Gong[2] and Ping Zhang[1]*

[1]Department of Dermatology, Traditional Chinese and Western Medicine Hospital of Wuhan, Tongji Medical College, Huazhong University of Science and Technology, Wuhan, China, [2]Department of Hepatobiliary Surgery, Traditional Chinese and Western Medicine Hospital of Wuhan, Tongji Medical College, Huazhong University of Science and Technology, Wuhan, China, [3]School of Materials and Science and Engineering, WuHan Technology of University, WuHan, China

Photodynamic therapy (PDT) is regarded as an alternative anti-tumor therapy which involves the administration of photosensitizers (PSs) and irradiation with specific light. However, conventional PDT therapy has been limited to the efficiency of PS delivery. A nanocarrier system could provide an effective platform for PS delivery and improve the efficiency of antitumor PDT. In this article, we prepared a complex consisting of aluminum phthalocyanine (AlPcS) and CdSe/CdZnS core-shell structure QDs and investigated the interaction between the complex and tumor cells. A more significant internalization of the conjugation was observed compared to free AlPcS *via* confocal fluorescence imaging. The tumor cells exhibited an obvious apoptotic trend after QD−AlPcS-mediated PDT.

KEYWORDS

cellular uptake, PDT, aluminum phthalocyanine, QDs, nanocarrier

Introduction

While Oscar Raab claimed that the interaction of acridine and light-rendered infusoria is fatal (Ackroyd et al., 2001), photodynamic therapy (PDT) has been used safely and successfully for 100 years (Rkein and Ozog, 2014). PDT entails the administration of photosensitizers (PSs) which can be excited by a certain wavelength of light and then generate singlet oxygen (Ochsner, 1997). Ultimately, this series of reactions leads to the apoptosis and necrosis of target cells with minimal detrimental effects on the adjacent tissue. Topical PDT has successfully evolved into an effective therapy for skin disorders such as for actinic keratosis (AK), squamous cell carcinoma (SCC), and basal cell carcinoma (BCC) (Naidoo et al., 2019). More recently, PDT has not

only been applied to treat benign skin disorders but has also been an alternative treatment for malignant melanomas. There have been many attempts to design new photosensitizers for anti-melanoma PDT (Baldea et al., 2018). Over recent decades, with the development of the biochemical industry, PDT has spread beyond the realm of dermatology and is currently used as an adjuvant therapy to treat disease at deeper sites, especially for hepatocellular carcinoma (HCC) when the situation is not suitable for other therapeutic strategies (Agostinis et al., 2011). Numerous studies have revealed that most PDT tactics could induce sufficient HCC cell death to meet clinical demand through apoptotic pathways, even though these are mediated by different photosensitive agents (Date et al., 2004; Yow et al., 2007). As a result of the oxidative stress brought on by PDT, local lesions are removed but cause severe acute inflammatory reactions and vascular damage *in vivo* (Bhuvaneswari et al., 2009). PDT thus offers an alternative treatment for solid tumors and demonstrates improved safeguarding of non-cancerous areas. This has been confirmed by *in vivo* research. Histological findings have demonstrated that PDT treatment inhibits tumor formation in tumor-implanted mice (Park et al., 2009). Wang et al. developed an efficient nanocarrier system for transporting IR780 and PTX, with the goal of effectively combining PTT/PDT with chemotherapy to treat HCC (Wang et al., 2017). In addition, several preclinical and clinical investigations have shown that PDT can also alter adaptive immune response in a variety of ways which contribute to its long-term efficacy (Thong et al., 2007; Kabingu et al., 2009). Presently, PDT is viewed as an intraoperative adjuvant procedure during HCC resection (Kumar et al., 2021). Despite the great superiority of PDT anticancer therapy, this treatment is still not fully adapted to clinical settings due to insufficient knowledge about PSs. The development of these is one of the most primary elements of PDT that enables it to operate more effectively. Accordingly, it is essential to improve the properties of PSs. In order to gain a comprehensive understanding about what constitutes ideal antitumor PSs, we should start from the following aspects: 1) the wavelength of activation light: tunable absorption peak from the UV to the near-infrared spectral region; 2) sufficient singlet triplet quantum yield leading to high ROS production;. 3) effective cellular uptake; 4) a rapid clearance rate that minimizes side effects such as phototoxicity; 5) selective accumulation at target sites (Abrahamse and Hamblin, 2016).

Phthalocyanine (Pc)—which exhibits excellent photochemical properties, including a short photosensitive period and a broad absorption band—as the second generation would lead to an increase in irradiation depth. It has been demonstrated that metal phthalocyanine (MPcs) can produce more singlet oxygen with high quantum yields (Iqbal et al., 2015). However, the clinical application of phthalocyanine is limited by its hydrophobicity and its characteristic easy aggregation in aqueous systems. There have only been four

Pc-based PSs: photosens (sulphonated aluminum phthalocyanine), Pc4, zinc-phthalocyanine, and photocyanine, which are available for clinical use or trial in different countries (Sekkat et al., 2011; Jiang et al., 2014). Nanotechnology holds great potential for the future in circumventing major drawbacks in traditional phthalocyanine. Numerous nanoplatforms have been investigated so far for effective and targeted PS delivery, employing a variety of organic and inorganic nanomaterials (Hong et al., 2016).

Among multiple nanomaterials, quantum dots (QDs) have unique advantages. QDs as semiconductor nanocrystals belong to inorganic nanomaterials, with a diameter of 3~10 nm. By virtue of their outstanding optical properties—including high fluorescence intensity, broad absorption, and narrow emission spectra—the application of QDs has expanded across many fields, including biomedical imaging (Matea et al., 2017). With broad absorption and narrow emission spectral, QDs have strong tissue penetration, and they specifically identify tumor-related biomolecules to improve the accuracy of targeted diagnosis and treatment (Kumari et al., 2021). One particular property of QDs should be emphasized: they could serve as energy donors to interact with dye molecules to cause Fluorescence resonance energy transfer (FRET), which dramatically improves antitumor efficacy. (Martynenko et al., 2015). Tekdaş et al. developed different types of QD–Pc conjugates in DMSO and confirmed that QDs could absorb light and function as donors to transfer energy to Pc by FRET (Tekdaş et al., 2012). These QD–Pc composites with a new excitation window of 400–600 nm might be a potential singlet oxygen generator, which is crucial for increasing PDT's effectiveness (Ma et al., 2008). Subsequently, a variety of studies have been conducted into the new potential PSs based on QD–Pc. Li et al. developed the AlPcS–QD conjugates and demonstrated the promise of this novel method in killing the majority of KB cancer cells *via* FRET-mediated PDT (Li et al., 2012). Due to the significant two-photon absorption (TPA) cross-section, QDs are also crucial in two-photon excited PDT (TPE-PDT) (Dayal and Burda, 2008). Chou et al. utilized an 800-nm femto-second (fs) pulsed laser beam to irradiate QDs–AlPcS and tested its efficiency in HeLa and KB cells; their findings demonstrated that a TPE-mediated FRET mechanism could be a breakthrough for traditional PSs, which are limited to narrow absorption spectra(Chou et al., 2013). Gvozdev et al. synthesized a complex based on QDs–AlPcS in which human transferrin was covalently bonded; the hybrid complex revealed the increased efficiency of PDT *via* clathrin-mediated internalization (Gvozdev et al., 2019). There is no doubt that QDs provide more opportunity to combine the PSs with target molecules. The combination of QDs and AlPcS not only shows remarkable antitumor efficacy but also expands the scope of indications. Melanoma and HCC cells in this article represent superficial malignant tumors and visceral tumors, respectively. We synthesized core-shell

FIGURE 1
TEM images of QDs–Cys in aqueous media.
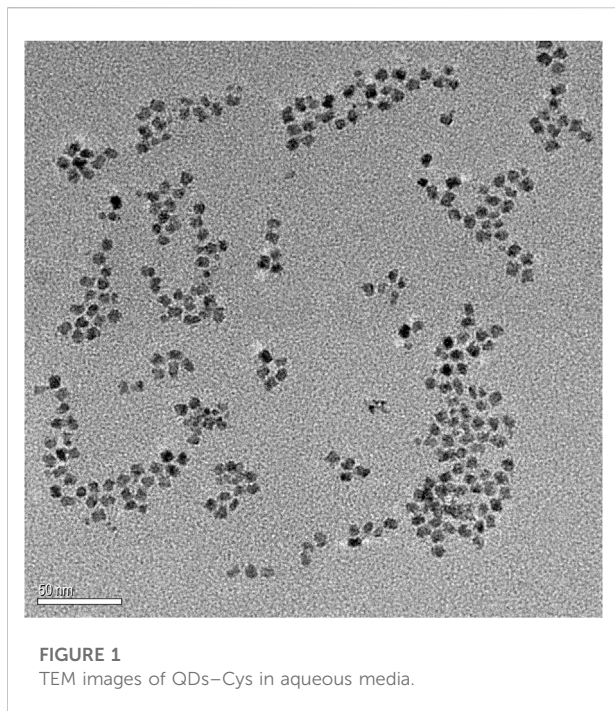
structure CdSe/CdZnS QDs for surface modification of aluminum phthalocyanine to improve hydrophobicity and measured the photophysical properties of the complex. We investigated the cellular uptake of the conjugation in melanoma and HCC cell models by confocal fluorescence images and quantified the fluorescent spot of intercellular conjugate using high-content microscopy. We then attempted to pinpoint the subcellular location of the conjugate using a lysosomal probe. Our findings demonstrate the potential of QD–AlPcS in PDT therapy and biomedical imaging. Cytotoxicity was determined by flow cytometry. This research could lay the foundation for future *in vivo* studies.

Methods and materials

Materials and instruments

Aluminum phthalocyanine (J&K chemical), CdSe/CdZnS QDs (synthesized by WuHan Technology of University Nano-materials Lab, emission wavelength 630 nm), L-arginine (Aladdin, 98%), 1,3-diphenylisobenzofuran (DPBF, Sigma-Aldrich, 97%), chloroform, formalin, and ethylalcohol (Sinopharm, AR). DMEM (Gibco), FBS (Gibco) PBS (TBD), 0.25% trypsase, Triton X-100, 5% BSA (Solarbio), Alexa Fluor 488-conjugated Affinipure Goat Anti-Rabbit (Bioswamp), ACTB Polyclonal Antibody (Bioswamp), LysoTracker Green DND-26 (Yeasen), Hoechst 33258 solution (Solarbio), ANNEXIN V-FITC (Solarbio), PI solution (Solarbio), confocal fluorescent microscopy (Leica TCS SP8), high-content microscopy (Perkin Elmer Operetta CLS), and cytomics flow cytometer (Beckman).

QD-AlPcS conjugation synthesis

CdSe/CdZnS core-shell structure QDs were prepared through pyrolysis (Xie et al., 2005). The final QD product was dispersed into trichloromethane. We poured a dose of L-Cys powder into deionized water and oscillated it for 30 min at 50°C and then added NaOH solution until the pH value ranged from 8 to 10. To this we added 2 ml QDs trichloromethane solvent and stirred for 2 h at room temperature until the solution turned from light yellow to no color. We then removed the trichloromethane solvent in the bottom of the tubes and put the upper QD solution into dialysis bags for 24 h to remove impurities, obtaining QDs–Cys solution. Because of the positive charge of the amine terminal, QDs could be dispersed in aqueous media and interact with the negatively charged AlPcS (there are four SO_4^{2-} in a benzene ring). We took a certain amount of QD–Cys solution and sulfonated AlPcS solution into tubes and oscillated them for 20 min. After 8 h reaction at room temperature, the solution was centrifuged at 8000 rpm for 5 min; we took the precipitate in the bottom of the tubes which resolved into PBS. Finally, a QD–AlPcS solution was obtained. The fluorescence emission spectrum was measured by using a spectrophotometer (QM-8000, Horiba), and the UV-vis absorption spectrum was also measured by using a spectrophotometer (UV-2550, SHIMADZU).

ROS assay

1,3-Diphenyliso-benzofuran (DPBF) is a commonly used $^1O_2$ indicator that quickly reacts with it. The production of ROS in a mixture solution will lead to the quenching of DPBF, so the singlet oxygen quantum yield was determined using DPBF as a probe. A mixture solution containing QDs-AIPcS (0.1 uM–5 uM), QDs (0.1 uM), AIPcS (5 uM), and DPBF (20 uM) was prepared. The test solution was illuminated with 405 nm light, and the spectral change of the test solution was recorded.

Cell culture

Huh-7 was purchased from Procell Life Technologies Inc. (Wuhan), A375 cells and B16 cells were purchased from the Chinese Academy of Science, and MIHA hepatic cells were given by the Department of Hepatobiliary Surgery at Xijing Hospital, Fourth Military Medical University. All cells were maintained in a 75-cm^2 cell culture dish in a humidified atmosphere at 37°C and 5% CO_2. Huh-7 cells and A375 cells were cultured in high glucose
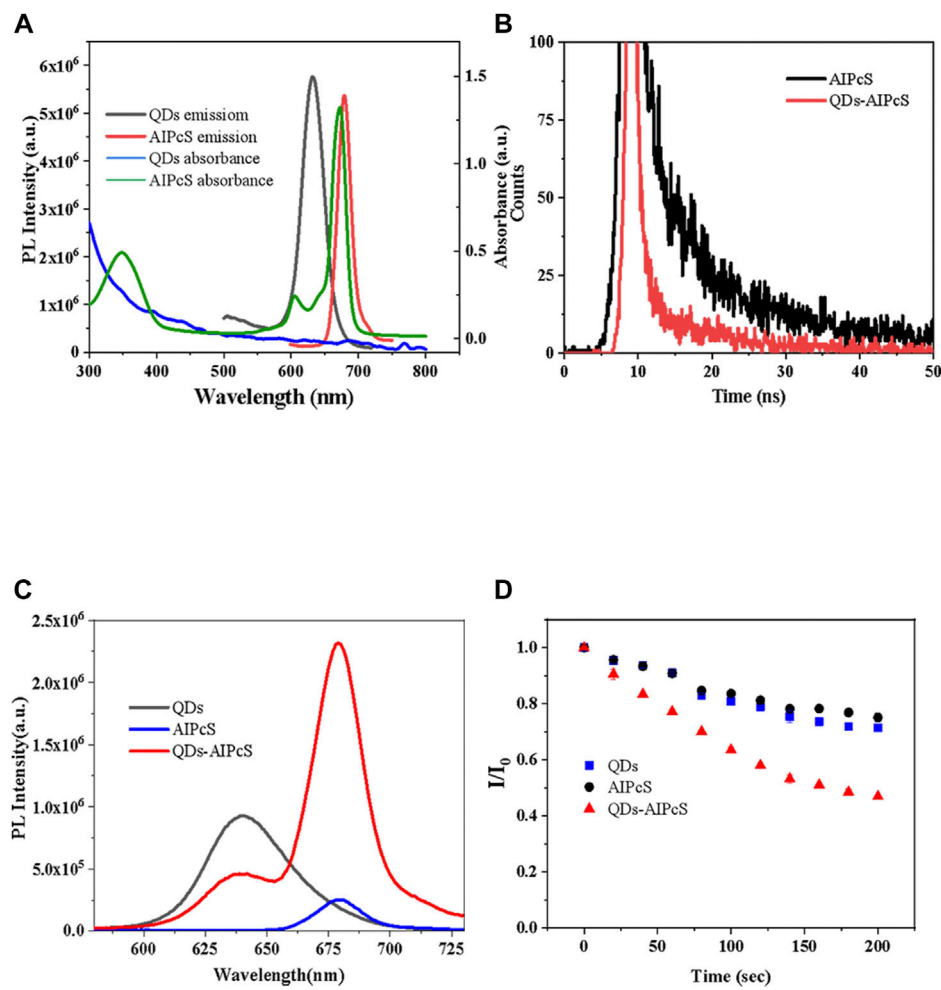
FIGURE 2
Photophysical properties of QDs, AlPcS, and QDs−AlPcS. **(A)** Absorption and emission spectrum of QDs and AlPcS. **(B)** PL life curves of QDs−AlPcS and free AlPcS excited by 400 nm light. **(C)** Fluorescence emission spectra of QDs−AlPcS, free QDs, and free AlPcS solution with excitation of 400 nm. **(D)** Comparison of DPBF photo-degradation in QDs−AlPcS, free QDs, and AlPcS solution.

Dulbecco's modified Eagle's medium (DMEM); the DMEM was supplemented with 10% fetal bovine serum and 1% penicillin/ streptomycin. The B16 cells and MIHA cells were cultured in PRMI-1640 with 10% FBS and 1% penicillin/streptomycin.

Confocal fluorescence images

When all cell types were passaged upon 80% confluency, the cells were incubated for 2 h in their respective growth media containing free QDs, free AlPcS, and QDs−AlPcS conjugates of varying concentrations (100 nm, 200 nm, 400 nm, and 1 μm). After incubation, the culture medium was removed and gently washed three times in 1 ml PBS, and 1 ml formaldehyde was then added. After 30 min fixation, the medium was washed once in PBS. For cell permeabilization, we added 1 ml 5‰ Triton X-100 and permeabilized for 15 min, and then rinsed it once in PBS. For cell closure, we added 1 ml 5% BSA solution and waited 1 h, and then rinsed twice in PBS. After closure, dried PBS, we added 1:400-actin antibody at 4°C overnight incubation. After three washes in PBS, we added 1: 400 secondary antibody containing FITC, incubated it for 1 h at 37°C, finished with three washes in PBS, and dyed it by DAPI. For the filter channel set, we excited 405 nm (FITC) and 488 nm (DAPI) at 405 nm and 488 nm wavelength laser. All fluorescence images were acquired under the same conditions and displayed at the same scale. B16 cells were seeded at 10^5 cells/dish in glass bottom dishes and incubated for 24 h. The old medium was replaced and washed twice with PBS . We then added fresh medium containing QDs−AlPcS
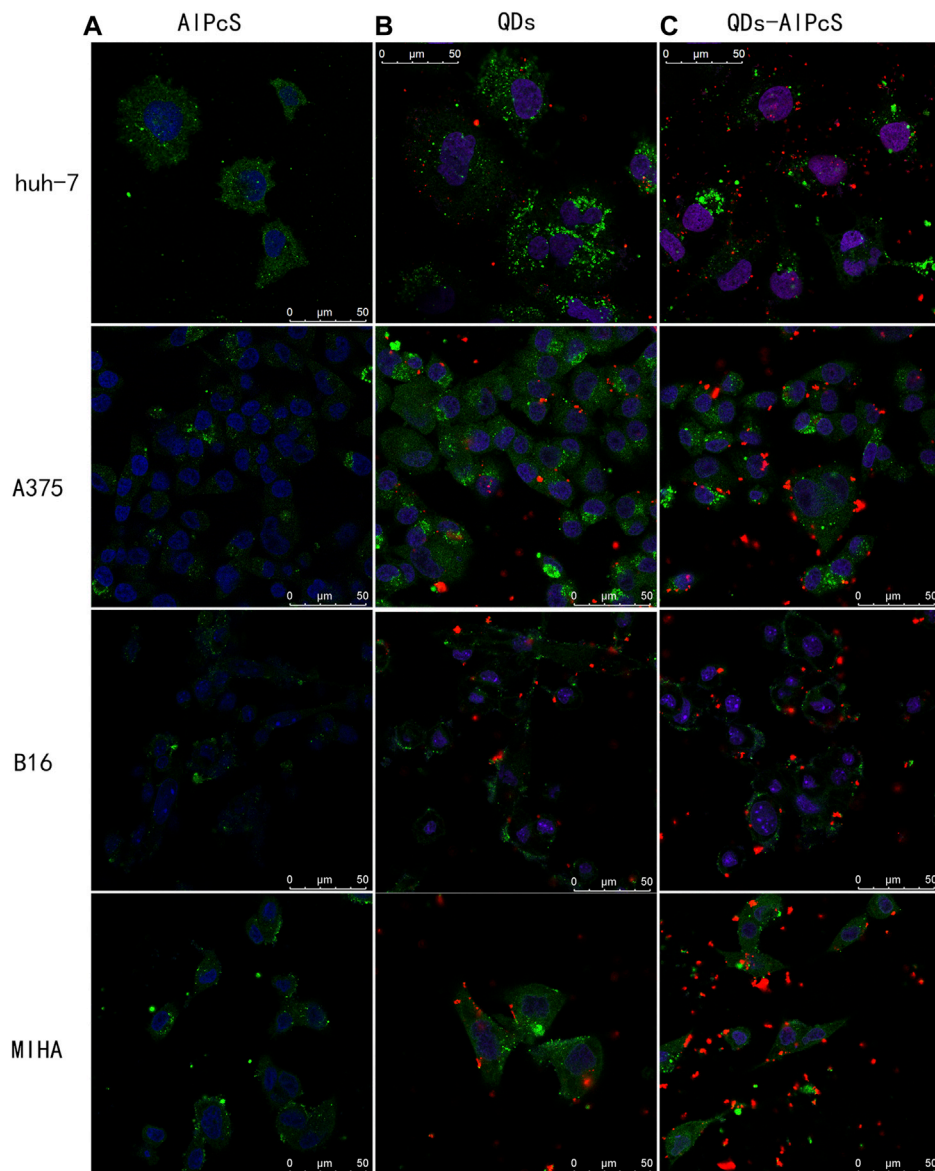
FIGURE 3
Confocal laser scanning microscopy image of four cell types incubated with three different materials for 2 h. The cytoskeleton was dyed green by FITC, and the nucleus was dyed blue by DAPI. The cells were incubated with the QD (0.4 uM) solution **(B)** and QD-AlPcS (0.4 uM–20 uM) solution **(C)** were excited by 405 nm laser light and exhibited red fluorescence in the picture. Cells incubated with free AlPcS (20 uM) solution **(A)** were irradiated with 638 nm laser light. Scale bar is 50 um.

incubated for another 2 h. After incubation, the cells were washed three times with PBS and incubated with 1 ml pre-warmed medium containing 100 nM LysoTracker Green DND-26 for 1 h. The medium containing LysoTracker was then replaced with 1% Hoechst 33258 staining solution. The cells were incubated in the staining solution for 30 min. The confocal microscopy images were obtained with Leica confocal microscopy.

Flow cytometry

The A375 and B16 cells were cultured in DMEM and PRIM1640 supplemented with QD–AlPcS conjugates for 2 h. After incubation, the culture medium was removed and gently washed once in 1 ml PBS; then, the samples were prepared following the Annexin V–FITC/PI cell death kit manufacturer's instructions of the Solarbio company. Flow
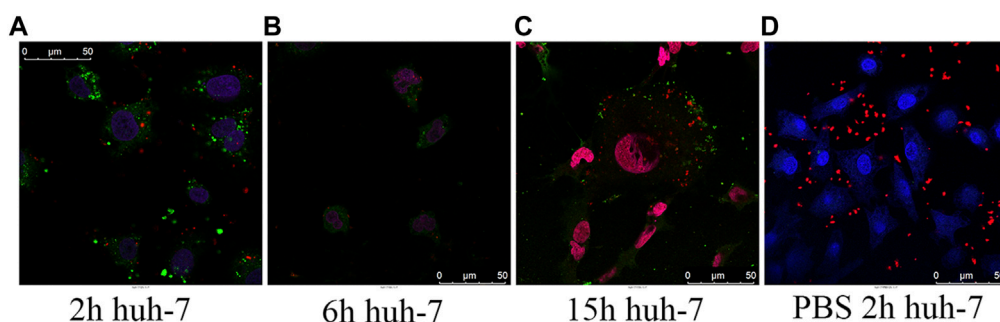
FIGURE 4
(A–C) Confocal laser scanning microscopy images of huh-7 cells incubated for 2 h **(A)**, 6 h **(B)**, and 15 h **(C)** in QD−AlPcS (0.4 uM−20 uM) DMEM solution; the cytoskeleton was dyed green by FITC, and the nucleus was dyed blue by DAPI. **(D)** Confocal laser scanning microscopy images of living huh-7 cells incubated in QDs−AlPcS PBS solution for 2 h, with cell nucleus dyed by Hoechst 33258. QDs−AlPcS conjugates were excited by wavelength of 405 nm and exhibited red fluorescence in the picture. Scale bar is 50 um.

cytometry analysis was conducted by using Cytomics Flow Cytometer 500 (Beckman-Coulter) with CXP software provided.

Results

Characterization of QDs and QDs−AlPcS conjugation

The complex consisting of QDs and AlPcS was synthesized by an electrostatic force in this study. To assess the linear dimension of the synthesized QDs, we utilized transmission electron microscopy (TEM). The TEM images are shown in Figure 1. The average diameter of the QDs was found to be 5−6 nm. The fluorescence emission and UV−vis absorbance spectra of free QDs and AlPcS in aqueous media are presented in Figure 2A. It can be observed that there is an obvious overlap between the absorbance spectra of AlPcS and the emission spectra of QDs in 600−700 nm, meaning that QDs as an energy donor has the potential to provide additional irradiation for AlPcS *via* the FRET process. In addition, in the 300−400 nm band, both AlPcS and QDs have absorbance peak. Thus, the fluorescence emission spectra of the QDs, AlPcS, and QDs−AlPcS solution under irradiation 400 nm are also presented in Figure 2C. The emission intensity (630 nm) of the conjugation decreased, while the emission intensity (690 nm) of the conjugation increased remarkably. This confirmed that the FRET mechanism works in the QD−AlPcS system. The efficiency of FRET between QDs and AlPcS was tested by the transient fluorescence spectrum of the complex and free AlPcS with irradiation of 400 nm light. As shown in Figure 2B, the FRET efficiency of the QDs−AlPcS complex reaches 57%. Singlet oxygen yield is an important parameter for assessing PDT efficiency. Here, DPBF was selected as the $^1O_2$ trapping agent; the $^1O_2$ yield was determined by measuring the changes in the PL

intensity of DPBF irradiated with 405 nm light. The PL intensity of DPBF decreased with irradiation time increasing (0~200 s) under irradiation of 400 nm. In Figure 2D, the DPBF quenching curves of the QDs−AlPcS mixture solution dropped more sharply than those of free QDs and the free AlPcS mixture solution. This implies that the conjugates produce more ROS through the FRET process, resulting in the degradations of DPBF reaching 70%.

Cellular uptake

The design of the NP-based delivery system emerges in an endless stream. The underlying endocytosis mechanism has attracted continuous attention, which plays an important role in improving the targeting efficiency of the NP-based agent (Zhang et al., 2015). In the current experiment, we utilized A375, B16, MIHA, and Huh-7 cell models to evaluate the cellular uptake and sub-localization of QDs−AlPcS. To gain an exhaustive comprehension of the effect of the interaction of the QDs−AlPcS conjugation with cancer cells, we first observed the cellular uptake or binding by taking the fluorescence images under the confocal laser scanning microscope (Leika TCS, SP8). In all types of cell model, red and spot-like fluorescence was observed in Figure 3. Stronger red fluorescence can be observed in the conjugation group compared to the free AlPcS group. There is no doubt that QDs could increase the cellular uptake of AlPcS. The Huh-7 cells incubated with the conjugation exhibited stronger red fluorescence than that of the human normal hepatic cell (MIHA), implying that cancer cells exhibit a higher affinity for QDs−AlPcS than normal cells. The cellular uptake of A375 and B16 cells was estimated the same way. Other than that, the results demonstrate that cellular exposure to increasing concentration and incubation time of the conjugation has a positive effect on cellular uptake. However, the morphology was gradually examined for signs of
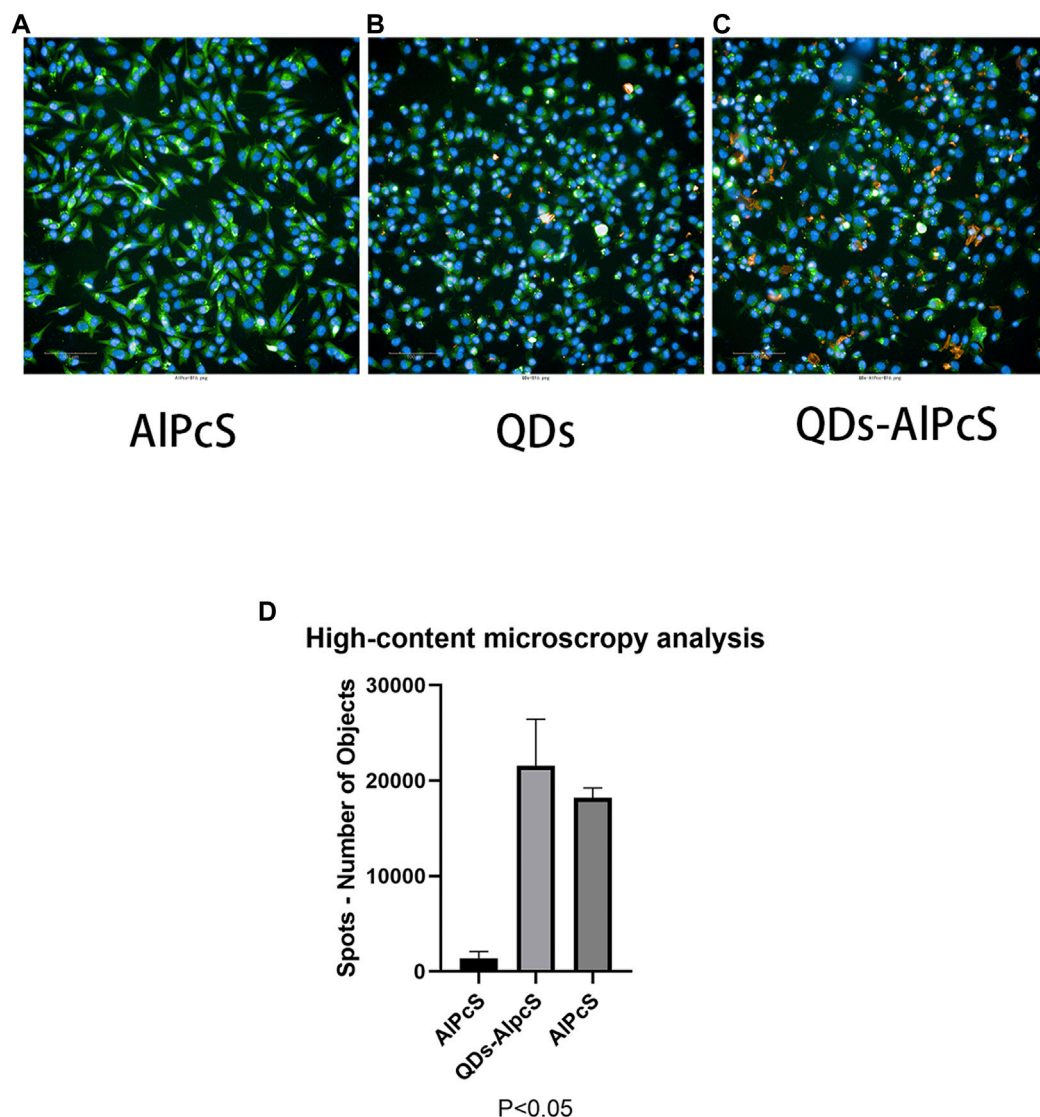
FIGURE 5
High-content microscopy images of B16 cells incubated for 2 h with free AlPcS **(A)**, free QDs **(B)**, and QDs−AlPcS **(C)** DMEM solution. Scale bar is 100 um. **(D)** Total amount of intracellular red fluorescence spots in a well of B16 cells which were incubated for 2 h with free AlPcS (20 uM), free QDs (0.4 uM−20 uM), and QDs−AlPcS (20 uM) DMEM solution. Data are shown by mean $\pm$ SD. $p < 0.05$ indicates significant difference, $n = 3$. Results calculated by GraphPad Prism 8.

apoptosis—such as cell shrinkage, membrane blebbing, and changes in intracellular architecture—as the incubating time increased, as seen in Figures 4A–C. It should be noted that there was no significant difference in fluorescence images when the concentration of QDs increased to 0.4 uM. This result is in line with a former study (Peng et al., 2013). During the experiment, an interesting phenomenon was found: the distribution of the conjugation had a tendency of encincturing the cellular contour. Furthermore, with the prolongation of incubation time, the red fluorescence spot of the conjugation converging from the peripheral region to the nucleus was more

marked. We then observed the samples under high-content microscopy analysis (Perkin Elmer Operetta CLS), which can obtain images of extensive vision and convert graphic to numerical data. We utilized this analysis system to calculate the intracellular red fluorescence spot of per well cells. The results of the QD-intervened group and the conjugation-intervened group are practically comparable in Figure 5D. Approximately, 90% cells could take up the conjugations and show red fluorescence under the microscope (Figures 5A–C).

Research has demonstrated that QDs without superficial functionalization could be transported by vesicle and localize
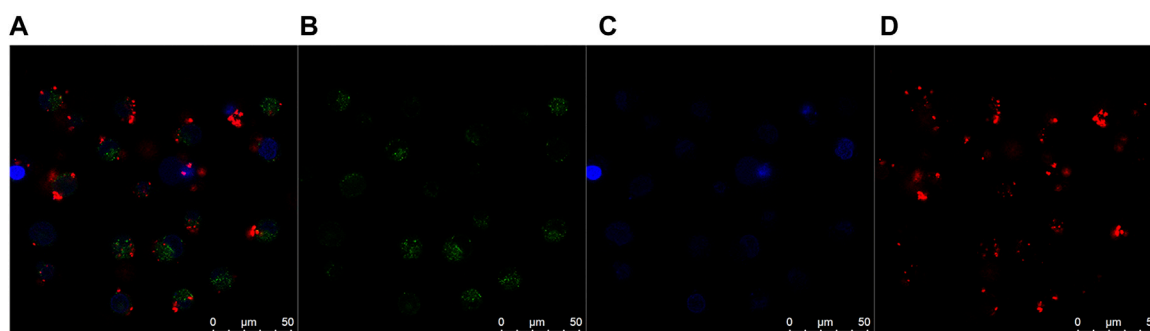
FIGURE 6
Confocal colocalization images of B16 cells incubated in QDs−AlPcS DMEM solution for 2 h. **(A)** Merges of three channels. **(B)** Lysosome labeled by LysoTracker Green DND-26 (green signals). **(C)** Nucleus dyed blue by Hoechst 33258. **(D)** Red fluorescence exhibited by QDs−AlPcS irradiated at 405 nm. Scale bar is 50 um.

in the lysosome (Jiang et al., 2010; Corazzari et al., 2013). Moreover, the endocytosis mechanism of QD-based nanomaterials has been much investigated. The results demonstrate that QDs conjugated with different biomolecules (including peptides, drugs, and penetration-promoting molecules) lead to different internalization pathways such as clathrin-mediated endocytosis and macropinocytosis-like endocytosis (Anas et al., 2009; Iversen et al., 2012). To further investigate the specific intracellular sub-localization of the conjugates, we utilized the lysosomal probe (LysoTracker Green DND-26). Confocal analysis provided evidence for co-localization of the particles (the red signals) and lysosomal (the green signals) in Figure 6, although the total co-localization rate is low at around 5–9%. Part of the QDs may be released from the QDs−AlPcS conjugation and localized in the lysosome. Those remaining may orientate to other organelles. The alteration can be attributed to the superficial functional molecules which lead to the varying endocytic mechanism.

Cytotoxicity assays of as-prepared QDs-AlPcS conjugation

The cytotoxicity of QDs is the main factor that influences their application. In order to investigate the phototoxicity of the QDs−AlPcS conjugation, flow cytometry was employed to evaluate cellular viability in our study. The cytotoxicity of the conjugation is, to a large extent, attributed to the QD component. The melanoma cells were exposed to QDs−AlPcS and 405 nm laser irradiation. As shown in Figure 7, cell viability decreased when irradiation and QDs−AlPcS collaborated to get the most of PDT. QDs−AlPcS (0.4 uM–20 uM) combined with 405 nm irradiation reduced melanoma cell viability by up to 40%. In contrast, QDs−AlPcS or 405 nm laser irradiation alone had no demonstrable influence on cell viability. These findings indicate

that PDT using a combination of QDs−AlPcS and a 405 nm laser has excellent cytotoxicity in melanoma cells. Similar research focusing on QDs has demonstrated that the cytotoxicity of QDs depends on size, composition, and superficial functionalization; the smaller size leads to greater toxicity (Clift et al., 2008; Maksoudian et al., 2020).

Discussion

In recent years, nanoparticles have gained much attention in clinical medicine due to their predominant biocompatibility and formability. Many studies have been conducted around designing a QD-based delivery system and biomolecule probe (Kim et al., 2012; Campbell et al., 2021). PSs can be modified directly by nanotechnology or delivered by nanocarrier to improve PDT efficiency and reduce side effects on normal tissues. NPs provide a versatile platform for PSs delivery (Kruger and Abrahamse, 2018). Currently, the nanoparticles commonly used for phthalocyanine modification include colloid gold, quantum dots, paramagnetic nanoparticles, silica-based materials, polymer-based nanoparticles, and carbonaceous tubules (Jia and Jia, 2012). Almost all modifications to phthalocyanine have aimed to improve its water solubility and targeting ability, and to generate more reactive oxygen species (ROS).

In this work, we chose CdSe/CdZnS QDs with 5 nm diameter as the nanocarrier for the intracellular delivery of AlPcS. To begin with synthesizing the conjugation, we found that AlPcS conjugating with QDs of higher concentration shows more obvious strengthened fluorescence. However, with increasing QDs concentration, the efficacy of FRET between AlPcS and QDs decreased. We then prepared a QDs−AlPcS conjugation at a 1:50 molar ratio (QDs/AlPcS) and measured the properties of the conjugation. The modified materials showed some parallels with unmodified QDs in
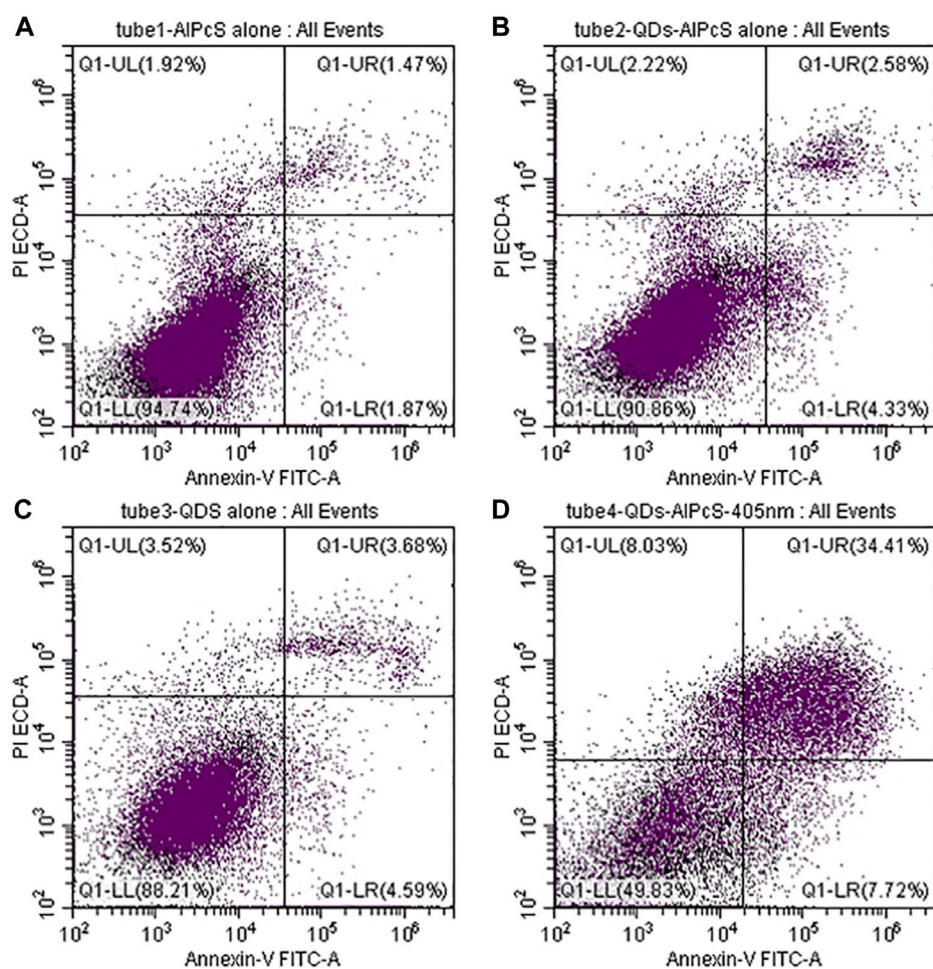
FIGURE 7
Cell death induction by QDs–AlPcS solution combined with 405 nm excitation in A375 cells. Q1-UL: necrotic cells (Annexin V negative/PI positive) Q1-UR: late apoptotic cells (Annexin V positive/PI positive) Q1-LL: viable cells (Annexin V negative/PI negative) Q1-LR: early apoptotic cells (Annexin-V positive/PI negative). **(A)** Cell viability of A375 cells incubated in free AlPcS (20 uM) solution without irradiation. **(B)** Cell viability of A375 cells incubated in QDs–AlPcS (0.4 uM−20 uM) solution without irradiation. **(C)** Cell viability of A375 cells incubated in free QDs (0.4 uM) solution without irradiation. **(D)** Cell viability of A375 cells incubated in QDs–AlPcS (0.4 uM−20 uM) solution with 405 nm irradiation.

cellular uptake analysis. In addition, previous research has shown that the cellular uptake of QDs is dependent upon incubation time at low concentration (Garcia-Calvo et al., 2021). The cellular uptake of QDs–AlPcS was investigated by confocal laser scanning imaging. Initially, the red fluorescence spot appeared around the cytomembrane. As the concentration increased, the opportunity for QDs–AlPcS attaching to the cytomembrane increased; the electrostatic force may promote this process. Endocytosis is an energy-consuming process. Based on this, we found that there is no cellular uptake when the incubating solution is PBS (Figure 4D). Some particles eventually localized in the lysosomes and were expelled, which may be attributed to the QDs released from conjugation. When it comes to application, biosafety

should be taken into account. The AlPcS conjugated with QDs by a liner-linkage structure, and QDs were enwrapped by many AlPcS molecules. The AlPcS acts as a shell-like role to protect the QD core. In theory, the complex leads to less influence on living cells: our *in vitro* results were consistent with this. Following the superficial functionalization of QDs, aggregation particles could be observed under a fluorescent microscope, particularly in a humidified atmosphere at 37°C for 6 h. The formation of aggregation particles hindered the endocytosis of QDs–AlPcS, and the efficacy of PDT had been influenced. We must therefore devise a strategy to overcome the aggregation problem. Regarding *in vivo* research, we have investigated the toxicity of the complex on tumor-bearing mice in the preliminary stages. After

intravenous injection, there is no obvious injury observed in tumor-bearing mice.

In conclusion, AlPcS is a promising photosensitizer but its application is limited due to its self-properties. QDs could serve as a carrier and an energy donor to enhance the delivery of AlPcS. In this work, we prepared the QDs–AlPcS conjugation and analyzed its cellular uptake and cytotoxicity by confocal microscopy and flow cytometry in four types of cell model. The results demonstrated that the internalization of AlPcS increases as a result of the concentrating excellence of QDs. The combination of QDs–AlPcS and 405-nm laser light exhibited a remarkable cell-killing effect *via* the FRET mechanism. Future research needs to explore the concrete endocytosis mechanism of QDs–AlPcS in the long term.

Data availability statement

The original contributions presented in the study are included in the article/Supplementary Material; further inquiries can be directed to the corresponding author.

Author contributions

All authors listed have made a substantial, direct, and intellectual contribution to the work and approved it for publication.

Conflict of interest

The authors declare that the research was conducted in the absence of any commercial or financial relationships that could be construed as a potential conflict of interest.

Publisher's note

All claims expressed in this article are solely those of the authors and do not necessarily represent those of their affiliated organizations, or those of the publisher, the editors, and the reviewers. Any product that may be evaluated in this article, or claim that may be made by its manufacturer, is not guaranteed or endorsed by the publisher.

References

Abrahamse, H., and Hamblin, M. R. (2016). New photosensitizers for photodynamic therapy. *Biochem. J.* 473 (4), 347–364. doi:10.1042/bj20150942

Ackroyd, R., Kelty, C., Brown, N., and Reed, M. (2001). The history of photodetection and photodynamic therapy. *Photochem. Photobiol.* 74 (5), 656–669. doi:10.1562/0031-8655(2001)074<0656:thopap>2.0.co;2

Agostinis, P., Berg, K., Cengel, K. A., Foster, T. H., Girotti, A. W., Gollnick, S. O., et al. (2011). Photodynamic therapy of cancer: An update. *CA A Cancer J. Clin.* 61 (4), 250–281. doi:10.3322/caac.20114

Anas, A., Okuda, T., Kawashima, N., Nakayama, K., Itoh, T., Ishikawa, M., et al. (2009). Clathrin-mediated endocytosis of quantum dot-peptide conjugates in living cells. *ACS Nano* 3 (8), 2419–2429. doi:10.1021/nn900663r

Baldea, I., Giurgiu, L., Teacoe, I. D., Olteanu, D. E., Olteanu, F. C., Clichici, S., et al. (2018). Photodynamic therapy in melanoma - where do we stand? *Curr. Med. Chem.* 25 (40), 5540–5563. doi:10.2174/0929867325666171226115626

Bhuvaneswari, R., Gan, Y. Y., Soo, K. C., and Olivo, M. (2009). The effect of photodynamic therapy on tumor angiogenesis. *Cell. Mol. Life Sci.* 66 (14), 2275–2283. doi:10.1007/s00018-009-0016-4

Campbell, E., Hasan, M. T., Gonzalez-Rodriguez, R., Truly, T., Lee, B. H., Green, K. N., et al. (2021). Graphene quantum dot formulation for cancer imaging and redox-based drug delivery. *Nanomedicine Nanotechnol. Biol. Med.* 37, 102408. doi:10.1016/j.nano.2021.102408

Chou, K. L., Won, N., Kwag, J., Kim, S., and Chen, J. Y. (2013). Femto-second laser beam with a low power density achieved a two-photon photodynamic cancer therapy with quantum dots. *J. Mat. Chem. B* 1 (36), 4584–4592. doi:10.1039/c3tb20928h

Clift, M. J., Rothen-Rutishauser, B., Brown, D. M., Duffin, R., Donaldson, K., Proudfoot, L., et al. (2008). The impact of different nanoparticle surface chemistry and size on uptake and toxicity in a murine macrophage cell line. *Toxicol. Appl. Pharmacol.* 232 (3), 418–427. doi:10.1016/j.taap.2008.06.009

Corazzari, I., Gilardino, A., Dalmazzo, S., Fubini, B., and Lovisolo, D. (2013). Localization of CdSe/ZnS quantum dots in the lysosomal acidic compartment of cultured neurons and its impact on viability: Potential role of ion release. *Toxicol. Vitro* 27 (2), 752–759. doi:10.1016/j.tiv.2012.12.016

Date, M., Fukuchi, K., Namiki, Y., Okumura, A., Morita, S., Takahashi, H., et al. (2004). Therapeutic effect of photodynamic therapy using PAD-S31 and diode laser on human liver cancer cells. *Liver Int.* 24 (2), 142–148. doi:10.1111/j.1478-3231.2004.00902.x

Dayal, S., and Burda, C. (2008). Semiconductor quantum dots as two-photon sensitizers. *J. Am. Chem. Soc.* 130 (10), 2890–2891. doi:10.1021/ja0781285

Garcia-Calvo, E., Cabezas-Sanchez, P., and Luque-Garcia, J. (2021). *In-vitro* and *in-vivo* evaluation of the molecular mechanisms involved in the toxicity associated to CdSe/ZnS quantum dots exposure. *Chemosphere* 263, 128170. doi:10.1016/j.chemosphere.2020.128170

Gvozdev, D. A., Ramonova, A., Slonimskiy, Y. B., Maksimov E, G., Moisenovich, M., and Paschenko, V. Z. (2019). Modification by transferrin increases the efficiency of delivery and the photodynamic effect of the quantum dot-phthalocyanine complex on A431 cells. *Arch. Biochem. Biophys.* 678, 108192. doi:10.1016/j.abb.2019.108192

Hong, E. J., Choi, D. G., and Shim, M. S. (2016). Targeted and effective photodynamic therapy for cancer using functionalized nanomaterials. *Acta Pharm. Sin. B* 6 (4), 297–307. doi:10.1016/j.apsb.2016.01.007

Iqbal, Z., Chen, J., Chen, Z., and Huang, M. (2015). Phthalocyanine-biomolecule conjugated photosensitizers for targeted photodynamic therapy and imaging. *Curr. Drug Metab.* 16 (9), 816–832. doi:10.2174/1389200217666151120165404

Iversen, T. G., Frerker, N., and Sandvig, K. (2012). Uptake of ricinB-quantum dot nanoparticles by a macropinocytosis-like mechanism. *J. Nanobiotechnology* 10, 33. doi:10.1186/1477-3155-10-33

Jia, X., and Jia, L. (2012). Nanoparticles improve biological functions of phthalocyanine photosensitizers used for photodynamic therapy. *Curr. Drug Metab.* 13 (8), 1119–1122. doi:10.2174/138920012802850074

Jiang, X., Rocker, C., Hafner, M., Brandholt, S., Dorlich, R. M., and Nienhaus, G. U. (2010). Endo- and exocytosis of zwitterionic quantum dot nanoparticles by live HeLa cells. *ACS Nano* 4 (11), 6787–6797. doi:10.1021/nn101277w

Jiang, Z., Shao, J., Yang, T., Wang, J., and Jia, L. (2014). Pharmaceutical development, composition and quantitative analysis of phthalocyanine as the photosensitizer for cancer photodynamic therapy. *J. Pharm. Biomed. Anal.* 87, 98–104. doi:10.1016/j.jpba.2013.05.014

Kabingu, E., Oseroff, A. R., Wilding, G. E., and Gollnick, S. O. (2009). Enhanced systemic immune reactivity to a Basal cell carcinoma associated antigen following photodynamic therapy. *Clin. Cancer Res.* 15 (13), 4460–4466. doi:10.1158/1078-0432.CCR-09-0400

Kim, M. J., Lee, J. Y., Nehrbass, U., Song, R., and Choi, Y. (2012). Detection of melanoma using antibody-conjugated quantum dots in a coculture model for

high-throughput screening system. *Analyst* 137 (6), 1440–1445. doi:10.1039/c2an16013g

Kruger, C. A., and Abrahamse, H. (2018). Utilisation of targeted nanoparticle photosensitiser drug delivery systems for the enhancement of photodynamic therapy. *Molecules* 23 (10), 2628. doi:10.3390/molecules23102628

Kumar, A., Moralès, O., Mordon, S., Delhem, N., and Boleslawski, E. (2021). Could photodynamic therapy Be a promising therapeutic modality in hepatocellular carcinoma patients? A critical review of experimental and clinical studies. *Cancers (Basel)*. 13 (20), 5176. doi:10.3390/cancers13205176

Kumari, A., Sharma, A., Sharma, R., Malairaman, U., and Singh, R. R. (2021). Biocompatible and fluorescent water based NIR emitting CdTe quantum dot probes for biomedical applications. *Spectrochimica Acta Part A Mol. Biomol. Spectrosc.* 248 (119206), 119206. doi:10.1016/j.saa.2020.119206

Li, L., Zhao, J. F., Won, N., Jin, H., Kim, S., and Chen, J. Y. (2012). Quantum dot-aluminum phthalocyanine conjugates perform photodynamic reactions to kill cancer cells via fluorescence resonance energy transfer. *Nanoscale Res. Lett.* 7 (1), 386. doi:10.1186/1556-276x-7-386

Ma, J., Chen, J. Y., Idowu, M., and Nyokong, T. (2008). Generation of singlet oxygen via the composites of water-soluble thiol-capped CdTe quantum dots-sulfonated aluminum phthalocyanines. *J. Phys. Chem. B* 112 (15), 4465–4469. doi:10.1021/jp711537j

Maksoudian, C., Soenen, S. J., Susumu, K., Oh, E., Medintz, I. L., and Manshian, B. B. (2020). A multiparametric evaluation of quantum dot size and surface-grafted peptide density on cellular uptake and cytotoxicity. *Bioconjug. Chem.* 31 (4), 1077–1087. doi:10.1021/acs.bioconjchem.0c00078

Martynenko, I. V., Kuznetsova, V. A., Orlova A, O., Kanaev, P. A., Maslov, V. G., Loudon, A., et al. (2015). Chlorin e6-ZnSe/ZnS quantum dots based system as reagent for photodynamic therapy. *Nanotechnology* 26 (5), 055102. doi:10.1088/0957-4484/26/5/055102

Matea, C., Mocan, T., Tabaran, F., Pop, T., Mosteanu, O., Puia, C., et al. (2017). Quantum dots in imaging, drug delivery and sensor applications. *Int. J. Nanomedicine* 12, 5421–5431. doi:10.2147/IJN.S138624

Naidoo, C., Kruger, C. A., and Abrahamse, H. (2019). Simultaneous photodiagnosis and photodynamic treatment of metastatic melanoma. *Molecules* 24 (17), 3153. doi:10.3390/molecules24173153

Ochsner, M. (1997). Photophysical and photobiological processes in the photodynamic therapy of tumours. *J. Photochem. Photobiol. B Biol.* 39 (1), 1–18. doi:10.1016/s1011-1344(96)07428-3

Park, K. C., Kim, S. Y., and Kim, D. S. (2009). Experimental photodynamic therapy for liver cancer cell-implanted nude mice by an indole-3-acetic acid and intense pulsed light combination. *Biol. Pharm. Bull.* 32 (9), 1609–1613. doi:10.1248/bpb.32.1609

Peng, L., He, M., Chen, B., Wu, Q., Zhang, Z., Pang, D., et al. (2013). Cellular uptake, elimination and toxicity of CdSe/ZnS quantum dots in HepG2 cells. *Biomaterials* 34 (37), 9545–9558. doi:10.1016/j.biomaterials.2013.08.038

Rkein, A. M., and Ozog, D. M. (2014). Photodynamic therapy. *Dermatol. Clin.* 32 (3), 415–425. x. doi:10.1016/j.det.2014.03.009

Sekkat, N., van den Bergh, H., Nyokong, T., and Lange, N. (2011). Like a bolt from the blue: Phthalocyanines in biomedical optics. *Molecules* 17 (1), 98–144. doi:10.3390/molecules17010098

Tekdaş, D. A., Durmuş, M., Yanık, H., and Ahsen, V. (2012). Photodynamic therapy potential of thiol-stabilized CdTe quantum dot-group 3A phthalocyanine conjugates (QD-Pc). *Spectrochimica Acta Part A Mol. Biomol. Spectrosc.* 93, 313–320. doi:10.1016/j.saa.2012.03.036

Thong, P. S., Ong, K. W., Goh, N. S., Kho, K. W., Manivasager, V., Bhuvaneswari, R., et al. (2007). Photodynamic-therapy-activated immune response against distant untreated tumours in recurrent angiosarcoma. *Lancet Oncol.* 8 (10), 950–952. doi:10.1016/S1470-2045(07)70318-2

Wang, D., Zhang, S., Zhang, T., Wan, G., Chen, B., Xiong, Q., et al. (2017). Pullulan-coated phospholipid and Pluronic F68 complex nanoparticles for carrying IR780 and paclitaxel to treat hepatocellular carcinoma by combining photothermal therapy/photodynamic therapy and chemotherapy. *Int. J. Nanomedicine* 12, 8649–8670. doi:10.2147/IJN.S147591

Xie, R., Kolb, U., Li, J., Basché, T., and Mews, A. (2005). Synthesis and characterization of highly luminescent CdSe-core CdS/Zn0.5Cd0.5S/ZnS multishell nanocrystals. *J. Am. Chem. Soc.* 127 (20), 7480–7488. doi:10.1021/ja042939g

Yow, C. M., Wong, C. K., Huang, Z., and Ho, R. J. (2007). Study of the efficacy and mechanism of ALA-mediated photodynamic therapy on human hepatocellular carcinoma cell. *Liver Int.* 27 (2), 201–208. doi:10.1111/j.1478-3231.2006.01412.x

Zhang, S., Gao, H., and Bao, G. (2015). Physical principles of nanoparticle cellular endocytosis. *ACS Nano* 9 (9), 8655–8671. doi:10.1021/acsnano.5b03184